Korean J. Chem. Eng., 37(5), 804-814 (2020)
DOI: 10.1007/s11814-020-0493-6

pISSN: 0256-1115
eISSN: 1975-7220

Effect of interfering ions on phosphate removal from aqueous media using magnesium oxide@ferric molybdate nanocomposite

Hossein Esmaeili*,†, Rauf Foroutan, Dariush Jafari*, and Mohammad Aghil Rezaei*****

*Department of Chemical Engineering, Bushehr Branch, Islamic Azad University, Bushehr, Iran
**Faculty of Chemical and Petroleum Engineering, University of Tabriz, Tabriz, 5166616471, Iran
***Department of Chemical Engineering, School of Chemical Engineering,
Kherad Institute of Higher Education, Bushehr, Iran
(*Received 3 November 2019 • accepted 12 January 2020*)

Abstract−The removal efficiency of phosphate ion from aqueous media using magnesium oxide/iron molybdate ($MgO/Fe_2(MoO_4)_3$) nanocomposite was investigated. MgO nanoparticles were chemically modified by ferric molybdate. Then, the structure and morphology of the nanocomposite was completely investigated using different analyses such as SEM, EDX/Map, FTIR, XRD, TGA, BET, and TEM. The TEM analysis demonstrated that the particles in the mentioned nano-composite were on a nanoscale. BET analysis proved that the nanocomposite was mesoporous with mean pore size of 9.4 nm. The sorption outcomes demonstrated that the highest phosphate sorption yield was achieved at 98.38%, exhibiting remarkable sorption efficiency. Carbonate ions showed to have the highest interfering impact compared to sulfate and nitrate ions, since phosphate ion removal efficiency decreased significantly when carbonate and phosphate ions were simultaneously available in the solution. The thermodynamic studies demonstrated that the current sorption process was spontaneous, possible, and exothermic. The sorption equilibrium investigation showed that the Freundlich isotherm model can describe the adsorption of phosphate ion better than can the Langmuir model, and the maximum sorption capacity was obtained as 30.21 mg/g. Additionally, the adsorbent was successfully regenerated four times and was able to perform the sorption and desorption process well.

Keywords: Magnesium Oxide/Iron Molybdate Nanocomposite, Phosphate Ion, Adsorption, Desorption

INTRODUCTION

Phosphate (P) is one of the most important chemicals that is widely used in the production of fertilizers, detergents, water softener agents, food and drink products, and other processes [1,2]. Based on the standards, the allowed phosphate concentration in drinking water is 0.5 mg/L, while its standard value for the wastewater discharge in surface waters is 5 mg/L [3]. Excessive phosphate content can cause serious problems, such as excessive growth and consequent bone injuries, high urea levels, asthma, nausea, kidney problems, anorexia, and the eutrophication of water resources [4]. Various processes have been used to remove phosphate from wastewater, including chemical precipitation [5,6], adsorption [7], biological methods [8], and reverse osmosis [9]. Most of these physical techniques, especially reverse osmosis, are expensive [9]. Among the above-mentioned methods, adsorption seems to be an appropriate method for treatment of wastewater containing contaminant due to the low-cost, simple, and high efficiency of sorbents [10]. In addition, the sorption capacities of the sorbents can be improved by activating their surfaces [11]. Previous studies have shown that some of the particles, such as iron, aluminum, zirconium, and titanium, are able to remove phosphate [12]. Generally, sorption is the process of removal of atoms and molecules from a liquid or gas phase in contact with a solid surface. Using this method, the dissolved organic chemicals and other harmful inorganic compounds are adsorbed on the adsorbent surface and can be separated from the aqueous media [13]. The most important adsorbent that has been used in this field is activated carbon [13], due to the high surface area, fast kinetics, high efficiency, and facile regeneration [14]. It has a large volume of dispersed pores with different sizes. Due to its considerable required time and cost of regeneration, activated carbon filters are usually installed along the other water treatment steps to promote the quality of the treated water. The efficiency of the adsorbent is dependent on its surface characteristics, so nano-adsorbents are being developed due to their high surface area. Therefore, several attempts have been made to design adsorbents with excellent efficiency, high selectivity, and stability. This is possible by modifying the pore size and shape, thermal and electronic structures, and chemical stability of these nanostructured materials [15].

The main aim of this study was to determine the phosphate ion sorption efficiency using $MgO/Fe_2(MoO_4)_3$ nanocomposite as a novel and efficient nano-sorbent. This nanocomposite was synthesized and used for the first time in this work. The mentioned adsorbent is a magnetic material that is easily removed from the solution by a magnetic field, which is one of the main advantages of this nanocomposite. Also, the characteristics of the nanocomposite were fully investigated by several analyses, such as SEM, EDX/Map, FTIR,

†To whom correspondence should be addressed.
E-mail: esmaeili.hossein@iaubushehr.ac.ir, esmaeili.hossein@gmail.com
Copyright by The Korean Institute of Chemical Engineers.

XRD, TGA, BET, and TEM. In this study, the effects of pH, sorbent dosage, process temperature, contact time, initial concentration of P and interfering ions on sorption efficiency of phosphate ion were examined. The adsorbent was reused and recovered. In addition, the sorbent behavior was investigated through kinetic, thermodynamic, and equilibrium studies of the sorption process.

EXPERIMENTAL

1. Chemicals

Dipotassium phosphate (KH_2PO_4) and nitric acid were purchased from Merck Company (Germany); iron nitrate nonahydrate and ammonium heptamolybdate were purchased from Biochem Company (France); and magnesium oxide was purchased from VCN Materials Company (Iran). In addition, the chemical reagent which was used to measure the phosphate ion concentration in aqueous solutions was synthesized by ammonium heptamolybdate (Biochem, France), ammonium monovanadate (Merck, Germany) and sulfuric acid (Merck, Germany). Note that pH adjustment of the phosphate ion samples was done with hydrochloric acid and sodium hydroxide 1 M, which were procured from Merck Company (Germany).

2. Preparation of Stock Solution

KH_2PO_4 was used to produce the stock solutions of P ion based on phosphorus. To this end, a specified amount of KH_2PO_4 (4.39 g) was added into 1 L of doubly distilled water to produce a solution containing 1,000 ppm P ion. The other phosphate solutions with appropriate concentrations were prepared by diluting the aforesaid stock solution. All experiments were done by using doubly distilled water.

3. Magnesium Oxide/Iron Molybdate ($MgO/Fe_2(MoO_4)_3$) Nanocomposite Synthesis

A 100 ml volumetric flask was used to synthesize the sorbent in which 0.327 g of iron nitrate nonahydrate was dissolved in 50 ml of doubly distilled water, then 0.5 g of magnesium oxide was added to it and blended for 30 minutes. The mixture temperature was enhanced to 80-90 °C; after that, ammonium heptamolybdate solution, which was acidified by nitric acid (pH=2), was gradually added and stirred for 3 hours. The achieved solution was then centrifuged at a rate of 3,000 rpm and stored at 105 °C for 24 hours to be completely dried. After drying, the sorbent was placed in a furnace at 500 °C for 10 hours. It was then powdered for further use in P sorption tests. The atomic ratio of molybdate to iron in the synthesized sorbent was 1.5 [16].

The surface characteristics of magnesium oxide/iron molybdate composite were specified using SEM, EDX/Map, FTIR, XRD, TGA, BET, and TEM analyses. The sorbent surface changes before and after the sorption process were analyzed using SEM analysis (HITACHI-S-3400), and EDX/Map analyses were employed to determine the constituent elements of the composite. The functional groups in the nano-composite were identified by FTIR (JASCO-460plus), while XRD (BRUKER D8) was applied to characterize the phases and crystallinity of the sorbent structure. TGA (Perkin Elmer S11) was also used to examine the thermal stability of the synthesized adsorbent. BET (Philips model, USA) analysis was applied to specify the surface structure and surface area of the aforementioned sorbent.

4. Adsorption Experiments

The sorption of P ions by magnesium oxide/iron molybdate nanocomposite was performed in batch mode. The impact of various factors such as pH value (2-10), sorbent dosage (0.2-2.5 g/L), temperature (25-50 °C), contact time (5-130 min), and phosphate ion concentration (10-70 mg/L) was investigated on sorption efficiency. The impact of interfering ions (0.01-0.1 mol/L), such as sulfate, nitrate, and carbonate ions, was checked on phosphate removal. The sorption capacity at equilibrium state (q_e) and sorption percent (R) was computed by Eqs. (1) and (2):

$$q_e = \frac{(C_i - C_e) \times V}{W} \tag{1}$$

$$R = \frac{C_i - C_e}{C_e} \times 100 \tag{2}$$

where C_i and C_e are initial and residual phosphate ion concentration (mg/L), W is the nanocomposite mass (g), and v is the sample volume (L).

The experiments were initially started by examining the effect of solution pH in the range of 2-10. To do this, 100 mL of the stock solution with the concentration of 20 mg/L was poured into a 250 mL Erlenmeyer flask. The sorbent dosage was also set in the range of 0.25-2.5 g/L. The sample was stirred using heater stirrer and the temperature and stirring rate was adjusted to 35 °C and 500 rpm, respectively. After 60 minutes, the phosphate ion concentration in the sample was measured using spectrophotometry. Using this data, the adsorption capacity and efficiency were calculated. The impact of other parameters was studied be changing the considered parameter, while the others were kept constant in the optimum values achieved in prior steps.

The chemical reagent which was used to measure the phosphate ion concentration by the spectrophotometer set was synthesized using ammonium heptamolybdate. To do this, 25 g of ammonium heptamolybdate was initially poured into a 175 mL volumetric flask and stirred to dissolve completely. Then, 280 mL of concentrated sulfuric acid was added to 400 mL of double distilled water and left to be cooled. Ammonium heptamolybdate solution was added and the volume of the achieved solution was increased to 1,000 mL using double distilled water. 2.5 g of $SnCl_2$-$2H_2O$ was dissolved in 100 mL glycerol (stannous chloride solution) and used as the reagent in the experiments. To perform the spectrophotometry tests, 50 mL of phosphate solution was blended with 2 mL of ammonium heptamolybdate solution and 0.25 mL of stannous chloride solution. The phosphate ion concentration in the aqueous solution was measured by spectrophotometer set at a wavelength of 690 nm.

5. Desorption and Regeneration of the Adsorbent

Desorption was studied by adding 2 g/L of $MgO/Fe_2(MoO_4)_3$ nanocomposite into 100 mL P ion solution with the concentration of 10 mg/L. The other conditions were kept constant (stirring rate of 500 rpm, pH value of 6, temperature of 45 °C, and contact time of 80 minutes). After the sorption tests, the aforementioned sorbent was separated from the aqueous media and washed twice by doubly distilled water to separate the precipitated P ions from its

surface. After washing, the adsorbent was added to 50 mL of sodium hydroxide solution (0.3 M) and stirred at different times (0.5-2.5 hr). The solution was filtered and the phosphate ion concentration was measured. Desorption tests were done for eight times, which showed the desorption capability of the synthesized composite. The desorption percentage can be computed using Eq. (3) [17]:

$$\text{Desorption (\%)} = \left(\frac{\text{amount of metal ions desorbed}}{\text{amount of metal ions adsorbed}}\right) \times 100 \qquad (3)$$

RESULTS AND DISCUSSION

1. Adsorbent Characterization

SEM and EDX/Map analyses were applied to investigate the structure of MgO nanoparticles and MgO/$Fe_2(MoO_4)_3$ nanocomposite before and after the phosphate ion adsorption, and their results are shown in Fig. 1. SEM images showed that MgO nanoparticles had a flat structure with different layers (Fig. 1(a)). EDX/Map analysis was used to determine the elements present on the MgO surface (Fig. 1(b) and (c)). It is quite revealing that oxygen and magnesium are uniformly distributed on the MgO surface with percentages of 43.01% and 56.99%, respectively. After preparing the MgO/$Fe_2(MoO_4)_3$ composite, there was considerable change in MgO surface by increasing the aggregation of particles. A possible explanation for this is the formation of MgO/$Fe_2(MoO_4)_3$ in MgO layers (Fig. 1(d)). EDX/Map analysis also showed that the content of oxygen and magnesium on the composite surface was decreased, while iron (12.11%) and molybdate (11.75%) were observed, indicating that $Fe_2(MoO_4)_3$ particles were formed (Fig. 1(e), (f)). After the phosphate sorption, the pores in the adsorbent were filled, possibly due to the sorption of P ions on the composite surface (Fig. 1(g)). The capability of MgO/$Fe_2(MoO_4)_3$ composite in P adsorption can be more accurately analyzed using EDX/Map technique. Fig. 1(h) and (i) reveal the presence of P ions (11.5%) on the aforementioned adsorbent.

The results of FTIR analysis on MgO nanoparticles and MgO/$Fe_2(MoO_4)_3$ nanocomposite before and after the adsorption of phosphate ions are presented in Fig. 2. It can be observed that there are intensive vibrations in MgO nanoparticles and MgO/$Fe_2(MoO_4)_3$ composite structures in the range of 3,438 and 3,436 cm^{-1}, respectively, which can be possibly attributed to the tensile vibrations of hydroxide groups in these materials [18]. There is also a peak at 1,630 cm^{-1} in MgO structure, which can be attributed to the bending vibrations of OH group [19]. In addition, the FTIR spectrum of MgO structure shows vibrations with different intensities at 859 cm^{-1}, 691 cm^{-1}, and 445 cm^{-1}, which correspond to the Mg-O-Mg vibration [19]. The ranges of sorption peaks in the MgO structure changed by the formation of MgO/$Fe_2(MoO_4)_3$ nanocomposite as the result of interactions between the groups present in MgO structure and iron and molybdate ions. Note that the

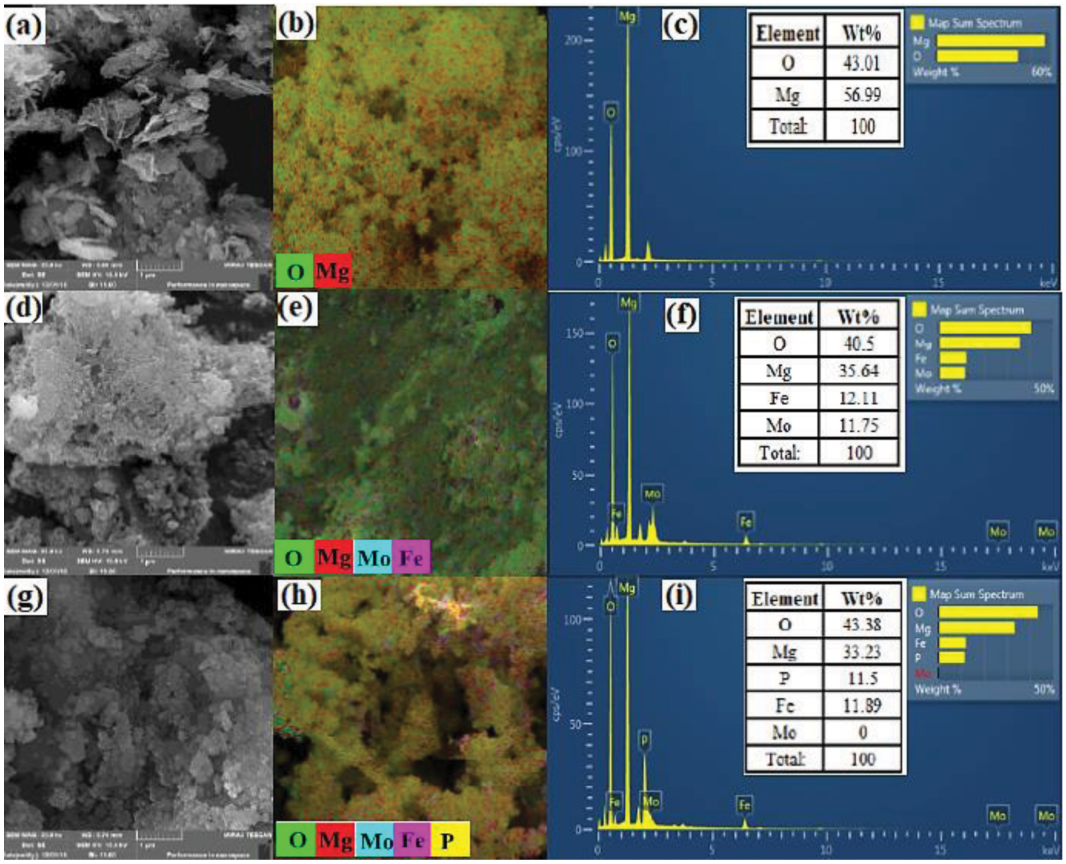


Fig. 1. Results of SEM and EDX/Map analyses for (a)-(c) MgO nanoparticles, (d)-(f) MgO/$Fe_2(MoO_4)_3$ nanocomposite, (g)-(i) MgO/$Fe_2(MoO_4)_3$ composite after the adsorption of P ions from aqueous media.

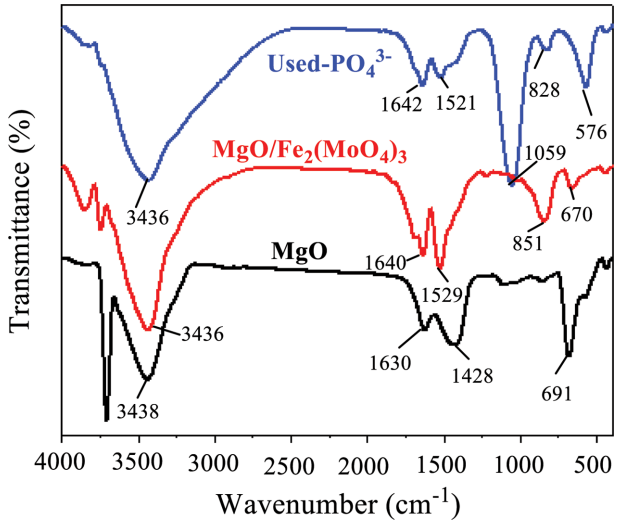


Fig. 2. FTIR analysis of MgO and $MgO/Fe_2(MoO_4)_3$ nanocomposite before and after phosphate ion adsorption.

$MgO/Fe_2(MoO_4)_3$ composite structure has a sorption peak at 851 cm^{-1} which was not observed in MgO structure. This can be attributed to the vibrations of different types of molybdate (Fe-O-Mo and FeMo) [20]. The peak at 445 cm^{-1} was a result of Mg vibration, which was transferred to 454 cm^{-1} after the synthesis of $MgO/Fe_2(MoO_4)_3$ composite as the result of magnesium and molybdate interactions and vibrations [21]. After the adsorption of P ions using $MgO/Fe_2(MoO_4)_3$ composite, the range of FTIR peaks changed and some new peaks were seen in the sorbent structure which are the results of P sorption on the applied composite. Furthermore, there are some other peaks at 1,059 cm^{-1} and 576 cm^{-1} which show v_3(P-O) and v_4(P-O) vibrations [22].

To identify the phases and also the crystallinity of MgO nanoparticles and $MgO/Fe_2(MoO_4)_3$ composite structures, XRD analysis was used. Fig. 3 reveals that there are various sharp peaks with different intensities in 2θ of 37.07°, 43°, 62.44°, 74.6°, and 78.78° in the MgO structure, which show (111), (200), (220), (311), and (222) crystalline phases in the MgO structure, in accordance with

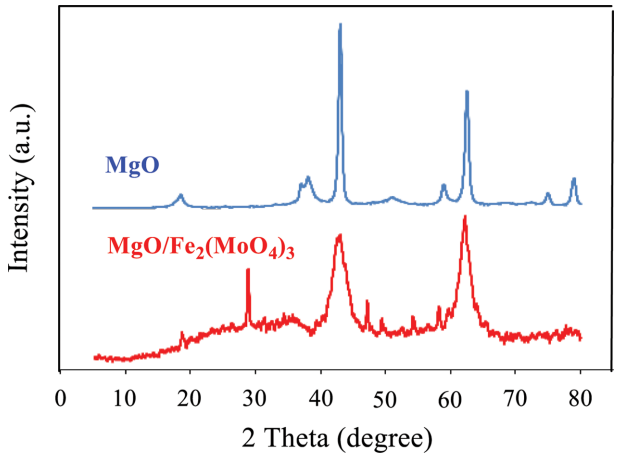


Fig. 3. XRD analysis of MgO and $MgO/Fe_2(MoO_4)_3$ nanocomposite.

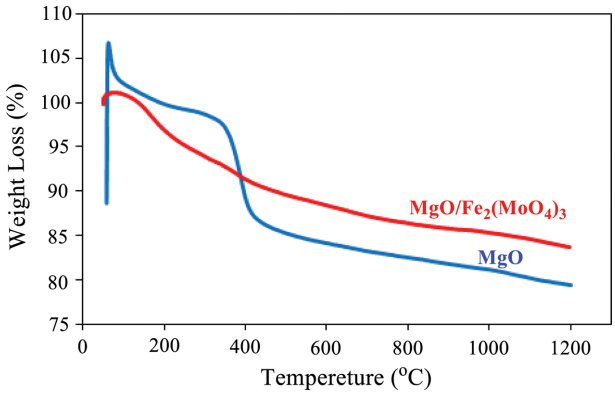


Fig. 4. TGA analysis for MgO and $MgO/Fe_2(MoO_4)_3$ nanocomposite.

JCPDS No. 77-2179 standard [23]. In addition, there is a single peak in 2θ=18.74° which can be related to $Mg(OH)_2$ [24]. After synthesis of $MgO/Fe_2(MoO_4)_3$ composite, the range of MgO peaks changed which, confirms the formation of $MgO/Fe_2(MoO_4)_3$ particles in MgO layers. In addition to MgO structure peaks, there are some other peaks in the structure of $MgO/Fe_2(MoO_4)_3$ composite in 2θ=24.72°, 27.88°, 28.74°, 41.96°, and 43.2°. These peaks are related to the crystalline phases of $MgO/Fe_2(MoO_4)_3$ composite, which accord with JCPDS No. 31-0642 standard [25]. In addition, the peaks observed in 2θ=94.32°, 53.2°, and 60.74° can be possibly expressed due to the presence of MoO_3 crystals in the synthesized adsorbent [25]. Generally, XRD results showed that $MgO/Fe_2(MoO_4)_3$ composite was successfully synthesized, and also MgO and $MgO/Fe_2(MoO_4)_3$ particles had crystalline structure.

Fig. 4 shows the TGA results that were applied to investigate the thermal stability of MgO and $MgO/Fe_2(MoO_4)_3$ composite. It can be observed that MgO and $MgO/Fe_2(MoO_4)_3$ samples lost their weight in the temperature range of 50-380 °C, which was the result of vaporization and humidity loss from the layers of mentioned samples that were physically adsorbed before [26]. The weight loss percentage of MgO and $MgO/Fe_2(MoO_4)_3$ samples was 5% and 6%, respectively. The second phase of weight loss occurred in 380-1,000 °C, where the corresponding values for MgO and $MgO/Fe_2(MoO_4)_3$ samples were 15% and 8%, respectively. This can be attributed to the degradation of MgO and $MgO/Fe_2(MoO_4)_3$ [27]. By increasing the temperature above 1,000 °C, there was a negligible weight loss (lower than 3%), which can be related to the final destruction of residuals of the mentioned samples.

The surface characteristics of MgO nanoparticles and $MgO/Fe_2(MoO_4)_3$ composite, including specific surface area, pore volume, and pore size, was evaluated using BET analysis. The specific surface area of MgO nanoparticles and $MgO/Fe_2(MoO_4)_3$ composite were determined as 154.92, and 2.55 m^2/g, respectively. Therefore, the specific surface area of the synthesized composite is significantly decreased compared to MgO nanoparticles, which is due to the presence of $Fe_2(MoO_4)_3$ nanoparticles within the layers and surface of MgO particles. Similarly, the pore volume for the composite (0.00599 cm^3/g) was significantly lower than MgO (0.219 cm^3/g), which confirms the formation of $Fe_2(MoO_4)_3$ nanoparticles in the layers and surface of MgO particles. Also, the average

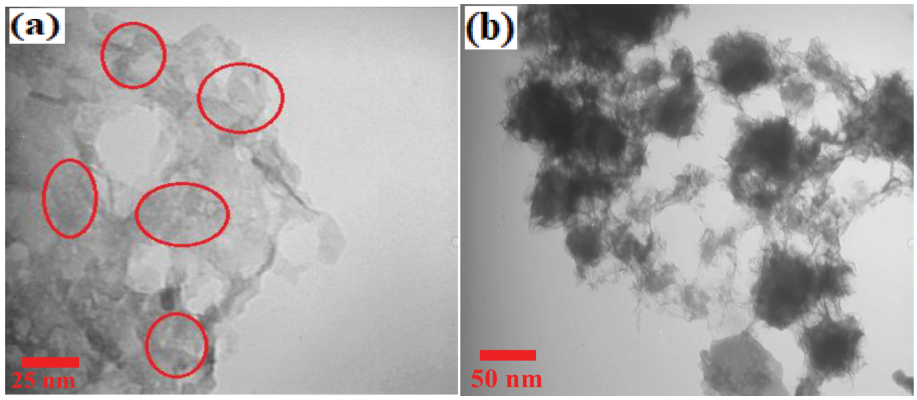


Fig. 5. TEM analysis for (a) MgO and (b) MgO/$Fe_2(MoO_4)_3$ nanocomposite.

pore diameter of MgO and MgO/$Fe_2(MoO_4)_3$ obtained 56.54 and 93.84 °A, respectively, which showed that both materials are mesoporous.

The results of TEM analysis for MgO nanoparticles and MgO/$Fe_2(MoO_4)_3$ composite are shown in Fig. 5. A flat structure with variable porosity can be obviously observed in Fig. 5(a), which is in accordance with SEM results. By the formation of MgO/$Fe_2(MoO_4)_3$ composite, significant changes can be seen in TEM images, which can be possibly related to the formation of $Fe_2(MoO_4)_3$ nanoparticles in the layers and surface of MgO particles. Consequently, the connections formed between MgO layers and $Fe_2(MoO_4)_3$ nanoparticles result in aggregation of particles and increasing their sizes. Note that the formation of $Fe_2(MoO_4)_3$ nanoparticles in the layers and surface of MgO particles was previously approved by SEM results.

2. Solution pH and Adsorbent Dosage Effects

Solution pH is one of the important factors affecting the removal of pollutants from wastewater using the adsorption process. Besides the effect of solution pH on the pollutant, it also changes the adsorbent surface charge by bombardment of the adsorbent surface using hydrogen and hydroxyl ions [28]. In the first stage in an acidic environment, the adsorbent surface is covered by the positive charge of hydrogen ions (H^+); meanwhile, it is saturated by the negative charge of hydroxyl ions (OH^-) in an alkaline environment. The second stage is attributed to the solution pH effect on phosphorus forms in acidic and alkali environments. Species of phosphate which exist in the aqueous media include zerovalent H_3PO_4 (phosphoric acid), monovalent $H_2PO_4^-$ (dihydrogen phosphate), divalent HPO_4^{2-}, and trivalent PO_4^{3-}. In an acidic medium where pH is lower than 4, the dominant species is H_3PO_4, which can be weakly connected to the adsorbent surface and eventually leads to low removal of phosphate ions from the aqueous solution. At pH between 5 and 10, the dominant phosphate species in the solution are $H_2PO_4^-$ and HPO_4^{2-}, which can be adsorbed on the active sites of the adsorbent. At these pH values, removal of phosphate ions probably occurs by the ion-exchange mechanism. At pH value above 10, the concentration of hydroxyl ions in the solution is high, and low removal of phosphate ions can be attributed to competition between OH^- ions and p ions for adsorbing on the active sites of the sorbent [29].

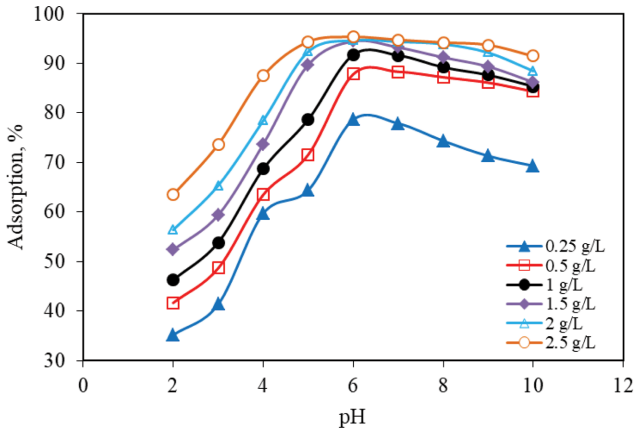


Fig. 6. The effect of solution pH and magnesium oxide/iron molybdate nanocomposite dosage on P ion sorption efficiency (initial phosphate concentration=20 mg/L, contact time=60 minutes, temperature=35 °C, and stirring rate=500 rpm). The mean value of standard deviation was 14.45%.

In the current work, the influence of solution pH and magnesium oxide/iron molybdate composite on the P ion sorption efficiency was investigated, and the results are presented in Fig. 6. Based on these data, the removal efficiency increased when pH was raised from 2 to 6. Because at acidic pH values (equal to 2), the dominant phosphorous form is phosphoric acid, which reduces the adsorption efficiency. By increasing pH to about 5-7, hydrogen phosphate ion becomes the dominant form, which results in the formation of strong bonds between this ion and the magnesium oxide/iron molybdate nanocomposite and the adsorption efficiency reaches a maximum value (pH=6). At pH>6, the sorption efficiency dropped as the result of the presence of P ions and competition between hydroxyl and phosphorous ions to adsorb on the surface of the composite. Consequently, the negative sorbent charge became higher which was followed by the desorption and precipitation of phosphorous ions from the adsorbent surface and reduced efficiency. Therefore, the highest sorption efficiency (94.64%) was achieved at pH=6.

The impact of magnesium oxide/iron molybdate composite dosage in the range of 0.25-2 g/L on the adsorption of phosphate ion

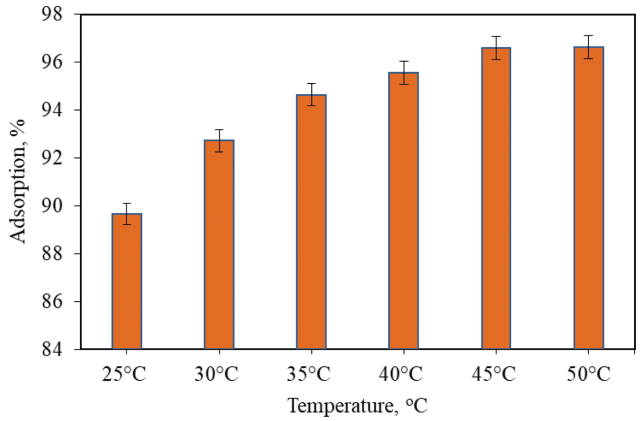


Fig. 7. The impact of temperature on P ions sorption efficiency using magnesium oxide/iron molybdate nanocomposite (initial phosphate ion concentration=20 mg/L, contact time=60 minutes, adsorbent dosage=2 g/L, and stirring rate=500 rpm). Relative standard deviation for these data was 2.46%.

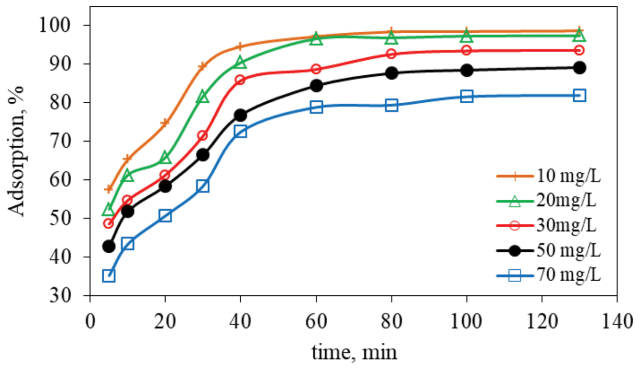


Fig. 8. The effect of initial P concentration and contact time on P ion sorption efficiency using magnesium oxide/iron molybdate nanocomposite (initial phosphate temperature=45 °C, adsorbent dosage=2 g/L, pH=6, and stirring rate=500 rpm). The standard deviation was less than 15% for all cases.

is presented in Fig. 6. As it is obvious, the phosphate ion adsorption efficiency declined initially and became 96.64% in the dosage value of 2 g/L. By increasing the dosage of the adsorbent, higher surface area and active sites are available for the adsorption of phosphate ions.

Also, the stability of the composite was investigated at different pH values. To measure molybdate, iron and magnesium ions in the aqueous solution after the adsorption of phosphate, the flame atomic absorption apparatus was used. The results showed that the mentioned composite was stable at different pH values and the amount of iron, molybdate and magnesium ions released into the solution was negligible (<0.24 mg/L).

So, the optimum value of pH and adsorbent dosage for the removal of phosphate ion from aqueous media using $MgO/Fe_2(MoO_4)_3$ nanocomposite was determined 6 and 2 g/L, respectively.

3. Temperature Effect

The impact of temperature on the adsorption of P ion which was studied in the range of 25-50 °C is presented in Fig. 7. As can be observed, higher temperatures promote the adsorption of phosphate on magnesium oxide/iron molybdate composite. Therefore, it can be concluded that the current adsorption process was endothermic and also ion exchange was desirable in higher temperatures. The increase in the adsorption efficiency of phosphate ions with increasing temperature can be related to the increase in the size of the adsorbent pores, change of its surface and diffusion of adsorbate across the external boundary layer [30]. In the same way, the compression of magnesium oxide/iron molybdate composite at lower temperatures leads in the reduction of pores volume. Overall, the utmost adsorption efficiency was 96.56%, which was achieved at 45 °C; and there was no sensible change in sorption efficiency at temperatures above 45 °C. Therefore, the optimum temperature for the adsorption of phosphate ion achieved was 45 °C.

4. Initial Ion Concentration and Contact Time Effects

The impacts of initial ion concentration and contact time on the sorption efficiency of phosphate ion by magnesium oxide/ferric molybdate nanocomposite can be observed in Fig. 8. An initial increase in slope demonstrates that the sorption of phosphate ion started at a quick rate and then continued slowly. In initial steps of adsorption, the adsorption rate was high because of the abundance of available active sites, but by approaching the equilibrium time (80 min), it slowed as a consequence of the occupation of adsorption sites by phosphate ions, which decreases the adsorption efficiency.

At lower initial concentration, the available adsorption sites were relatively higher and phosphate ions can be conveniently adsorbed on these sites. But when the concentration was increased the unsaturated active site was limited, and therefore there will be more phosphate ions remaining in the solution, which results in lower efficiency values. In addition, the ratio of pollutant to the active sites of the adsorbent was higher in lower initial concentrations; therefore, the adsorption was independent of this parameter, but the competition between the phosphate ions for the active sites was intensified at higher initial concentrations, which was followed by lower adsorption efficiencies. Based on the outcomes, the maximum sorption efficiency of phosphate ion (98.38%) was achieved at initial phosphate ion concentration of 10 mg/L and contact time of 80 min; after this time, the removal efficiency did not change significantly. Therefore, the initial concentration of 10 mg/L and contact time of 80 min were reported as the optimal values.

5. Ions Interference Effect on Adsorption Efficiency

Generally, the existence of some ions such as sulfate (SO_4^{2-}), nitrate (NO_3^-), and carbonate (CO_3^{2-}) in real sewages and surface waters affects the adsorption of pollutants. In this work, the presence of sulfate, nitrate, and carbonate ions in aqueous solutions and their effect on phosphate adsorption efficiency using $MgO/Fe_2(MoO_4)_3$ composite was investigated, and the results are shown in Fig. 9. Based on this figure, it can be observed that by changing the ion concentration from 0.01 M to 0.1 M, the phosphate adsorption efficiency declined from 98.14% to 94.47, 97.43% to 90.38%, and 94.21% to 66.73% for nitrate, sulfate, and carbonate ions, respectively. As is obvious, the decrease in adsorption efficiency was more significant for carbonate compared to the other two ions. Because sulfate and nitrate ions can occupy the active sites on the composite surface less than the carbonate ion, and car-

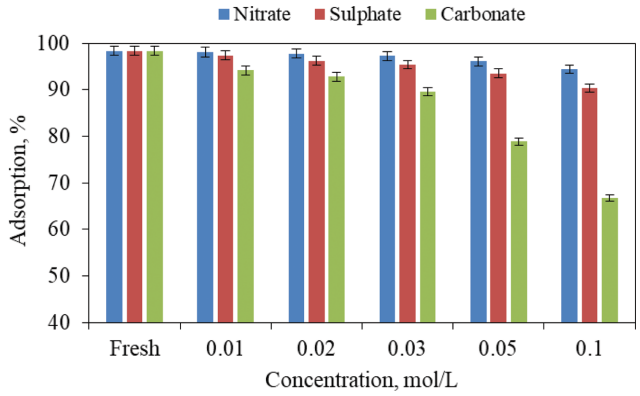


Fig. 9. Effects of interfering ions such as carbonate, sulfate, and nitrate on the P ion sorption using $MgO/Fe_2(MoO_4)_3$. The mean standard deviation was obtained 4.9%.

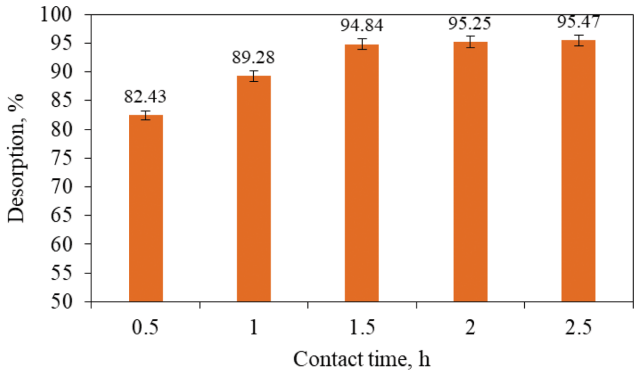


Fig. 10. The effect of contact time on the desorption of P ions using $MgO/Fe_2(MoO_4)_3$ nanocomposite. The standard deviation was 5.06.

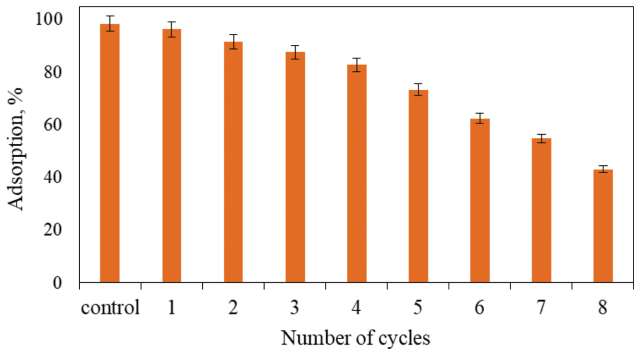


Fig. 11. Adsorption/desorption studies of P ions using $MgO/Fe_2(MoO_4)_3$ nanocomposite. The standard deviation was 16.88%.

bonate ion has a more interfering effect in the adsorption of phosphate ion from aqueous solution. Also, because of their negative charges, they prevent the easy adsorption of phosphate ions (PO_4^{3-}) on the adsorbent surface. The findings observed in this study mirror those of the previous studies that have shown the competition between carbonate and phosphate ions for adsorption on the adsorbent active sites [31].

6. Desorption Experiments and Reuse of the Adsorbent

The possibility and reusability of the adsorbents is a key factor for their industrial application. Desorption studies of the $MgO/Fe_2(MoO_4)_3$ nanocomposite after adsorption of phosphate ions were performed using NaOH solution (0.3 M) in different periods of time, and the results are shown in Fig. 10. The findings observed in this figure show that phosphate ion desorption percentage from the synthesized composite decreased with time and the maximum desorption percentage was 94.84%, which was achieved after 1.5 hr.

Also, the reusability of the aforementioned composite was studied in eight stages of sorption/desorption, and the results are demonstrated in Fig. 11. The decrease of sorption efficiency of $MgO/Fe_2(MoO_4)_3$ composite for the phosphate sorption from aqueous media was lower than 5% after four stages of sorption/desorption process. Then, the decrease in adsorption capacity was significant, which can be related to the competition between OH^- and phosphate ions for sitting on the adsorbent surface [32]. The most striking result to emerge from these data is that $MgO/Fe_2(MoO_4)_3$ composite can be used for four stages of sorption/desorption process of phosphate ion and can be considered as an appropriate one for the removal of this contaminant.

7. Comparing the Results with Previous Studies

The adsorption of phosphate ion from aqueous media by using the adsorbent used in this study and other adsorbents used in the literature was compared, and the result is presented in Table 1. As shown, the maximum adsorption capacity and the removal efficiency of phosphate ion obtained in this work were comparable to

Table 1. Comparing the results with previous studies

Adsorbent	Temperature (°C)	pH	Time (h)	Adsorbent dose (g/L)	Phosphate dose (mg/L)	Removal efficiency (%)	q_{max} (mg/g)	Ref.
MgO/Fe_3O_4	25	9	20 min	5	1	98.9	2.95	[5]
Modified giant reed	20	5	1	16	50	98	34.6	[29]
Molybdate/brown algae	50	5	1	10	30	98.7	149.25	[33]
Alginate/geothite	20	4	2	10	10	97.6		[34]
Geothite	20	4	2	10	10	70		[34]
Raw peat	-	-	-	-	-	-	0.92	[35]
Iron-modified peat	20	2	24	12.5	50	99.5	11.53	[35]
Iron oxide tailings	-	-	-	-	-	-	8.21	[36]
$MgO/Fe_2(MoO_4)_3$	45	6	1 h 20 min	2	10	98.38	30.21	Present study

previous studies. In this study, the removal efficiency of 98.38 was obtained at the adsorbent dosage of 2 g/L and contact time of 80 min, which in comparison to the previous studies was achieved at less contact time and lower adsorbent dosage. Therefore, the results show that the adsorbent used in the present study is more efficient than the other adsorbents in the removal of phosphate ion from aqueous media.

8. Equilibrium Isotherm Study

Adsorption isotherm models are usually applied to define the sorption process and its mechanism. Freundlich, Langmuir, and Dubinin-Radushkevich isotherms are well-known models which are extensively used in this research. In the Langmuir model, it is assumed that sorption occurs on a single and homogeneous layer of the sorbent surface. The linear form of the Langmuir equation is given as below:

$$\frac{C_e}{q_e}=\frac{1}{K_L q_m}+\frac{C_e}{q_m} \tag{4}$$

where C_e is the equilibrium concentration of phosphate ion (mg/L) and q_e is the amount of phosphate ion adsorbed in equilibrium state per gram of the sorbent. Also, q_m is the maximum amount of the contaminant adsorbed per gram of the sorbent (mg/g), and K_L is the Langmuir constant which depends on the adsorbent sites (L/mg). Langmuir constants, q_m and K_L, are achieved from the slope and intercept of C_e/q_e versus C_e plot. In addition, the sorption intensity (R_L) is a dimensionless parameter and is defined as follows [37].

$$R_L=\frac{1}{1+K_L C_i} \tag{5}$$

where C_i is the contaminant concentration at initial time (mg/L). The desirability value of the adsorption process can be determined through the value of R_L. If $0<R_L<1$, $R_L>1$, $R_L=1$, $R_L=0$, the process is categorized as desirable, undesirable, linear, and irreversible, respectively [15].

The Freundlich isotherm model is used for heterogeneous surfaces and multilayer adsorption of pollutants on the adsorbent surface. The linear form of this model is described as follows:

$$\ln q_e=\ln K_f+\frac{1}{n}\ln C_e \tag{6}$$

In this equation, K_f (L/mg) and n are Freundlich constants which are used to express the adsorption amount. If n=1, the process is linear. Furthermore, n<1 and n>1 show that the adsorption processes are unfavorable and favorable, respectively.

Dubinin-Radushkevich is an isotherm model that has been used in this work to determine the chemical or physical nature of the phosphate ions adsorption from the aqueous solution. The linear form of this model is described as follows:

$$\ln q_e=\ln q_{max}-\beta\varepsilon^2 \tag{7}$$

where β and ε are Dubinin-Radushkevich isotherm constant (mol^2/kJ^2) and Polanyi potential (kJ/mol). Parameter ε can be calculated using the following equation:

$$\varepsilon=RT\ln\left(1+\frac{1}{C_e}\right) \tag{8}$$

where T and R are temperature (K) and the universal gas constant. In addition, β is used to calculate the adsorption mean free energy, (E) (kJ/mol), which is defined as follows:

$$E=\frac{1}{\sqrt{2\beta}} \tag{9}$$

where E describes the adsorption mechanism (physical or chemical). For E values between 8 and 16 kJ/mol, the adsorption process is chemical adsorption; if this parameter is lower than 8 kJ/mol, the process has a physical nature [38].

As mentioned, Langmuir, Freundlich, and Dubinin-Radushkevich isotherms were used to investigate the adsorption of phosphate ions on $MgO/Fe_2(MoO_4)_3$ composite. The results of equilibrium study are illustrated in Fig. S1 and their constants and parameters are reported in Table 2.

The maximum adsorption capacity using the Langmuir isotherm model achieved was equal to 30.211 mg/g and R_L was obtained in the range of 0.023-0.114 ($0<R_L<1$), which denotes that the adsorption process was desirable. In addition, the amount of

Table 2. Estimated parameters for Langmuir, Freundlich, and Dubinin-Radushkevich models in the adsorption of P ion on the surface of $MgO/Fe_2(MoO_4)_3$ nanocomposite

Models	Parameters	Adsorbent
		$MgO/FeMoO_4$
Langmuir	q_m (mg/g)	30.211
	K_L (L/mg)	0.5932
$C_e/q_e=C_e/q_m+1/K_Lq_m$	R^2	0.9835
	R_L	0.023-0.144
Freundlich	n	2.619
$\ln q_e=\ln K_f+1/n \ln C_e$	K_f ($mg\cdot L^{1/n}/g\cdot mg^{1/n}$)	10.488
	R^2	0.9907
Dubinin-Radushkevich (D-R)	E (KJ/mol)	3.0686
	q_m (mg/g)	19.026
$\ln q_e=\ln q_m-\beta\varepsilon^2$	$\beta\times10^{-6}$ (mol^2/J^2)	0.0531
	R^2	0.8084

Table 3. Kinetic parameters for the adsorption of P ion on $MgO/Fe_2(MoO_4)_3$ nanocomposite

Kinetic model	Parameters	Concentration phosphate ions				
		10 mg/L	20 mg/L	30 mg/L	50 mg/L	70 mg/L
Quasi first-order	R^2	0.9841	0.9693	0.9585	0.9257	0.9683
	K_1 (1/min)	0.0633	0.065	0.059	0.0397	0.0503
	$q_{e.cal}$ (mg/g)	3.083	8.359	13.58	15.78	26.151
	$q_{e.exp}$ (mg/g)	4.931	9.738	14.034	22.285	28.661
Quasi second-order	R^2	0.999	0.9975	0.9967	0.9971	0.9955
	K_2 (g/mg·min)	0.038	0.0137	0.0074	0.0042	0.0027
	$q_{e.cal}$ (mg/g)	5.165	10.38	15.12	24.09	31.54
	$q_{e.exp}$ (mg/g)	4.931	9.738	14.034	22.285	28.661
Intra-particle diffusion	K_i (mg/g·$min^{1/2}$)	0.2296	0.5246	0.8122	1.3417	1.9148
	I (mg/g)	2.7749	4.7358	6.1064	9.0399	9.915
	R^2	0.8025	0.8471	0.8889	0.9165	0.8929

heterogeneity of the adsorbent surface, n, obtained was 2.619, which shows the adsorption process is favorable and physical.

Since most of the applied adsorption isotherms cannot calculate the reaction energy, Dubinin-Radushkevich isotherm was used to determine the adsorption energy and type of adsorption reaction by the calculation of Polanyi potential (Fig. S1(c)). As can be seen in Table 2, q_{max} and β are 19.026 mg/g and 0.0531 mol^2/J^2, respectively. Based on the values of these parameters, the adsorption energy was 3.069 kJ/mol, which shows that the adsorption of phosphate ions on the $MgO/Fe_2(MoO_4)_3$ composite is physical.

Also, the results showed that the Freundlich isotherm model was better fitted with the experimental data for describing the adsorption of phosphate ions, because its correlation coefficient was the highest value (R^2=0.991) compared to the Langmuir (R^2=0.9835) and Dubinin-Radushkevich (R^2=0.8084) models. Therefore, it can be said that the adsorption of phosphate ions occurred on the multilayer and heterogeneous surface of $MgO/Fe_2(MoO_4)_3$ composite. Also, the correlation coefficient for the Dubinin-Radushkevich model was 0.8084, which shows this model has a significant difference with the experimental data and it's not appropriate to describe the equilibrium behavior of the adsorption process. Similar results are seen in previous studies [39,40].

9. Adsorption Kinetics

Adsorption kinetics includes several stages, such as the transfer of pollutant to the adsorbent surface, its transfer from surface to the intramolecular active sites, and the retention of adsorbed particles in active sites by adsorption, sedimentation, and complex formation. To this end, quasi-first-order, quasi second-order, and intra-particle diffusion kinetic models were used to illustrate the kinetic behavior of the sorption process. The linear forms of the quasi-first and quasi-second-order models are presented as Eqs. (10) and (11), respectively [13,14]:

$$\ln(q_e - q_t) = \ln q_e - K_1 t \tag{10}$$

$$\frac{t}{q_t} = \frac{1}{K_2 q_e^2} + \frac{t}{q_e} \tag{11}$$

where t and q_t are contact time (min) and the sorption capacity at time t (mg/g), respectively. Moreover, K_1 and K_2 are the quasi-first-order (min^{-1}) and quasi-second order (g/mg·min) kinetics rate constant, respectively.

To analyze the adsorption mechanism of the adsorbent, the intra-particle diffusion model was used. This model provides a more accurate idea of the adsorption mechanism of pollutants on the adsorbent surface, compared to the pseudo-first order and the pseudo-second order models. The linear form of the intra-particle diffusion model can be expressed as follows:

$$q_t = K_i t^{1/2} + I$$

where K_i (mg/g·$min^{1/2}$) represents the intra-particle diffusion rate constant, and I (mg/g) gives information about the thickness of the boundary layer [41].

The results of kinetics study of phosphate ion sorption using magnesium oxide/ferric molybdate composite are presented in Fig. S2 and Table 3. Based on the data presented in Table 3, it can be obviously observed that the predicted sorption capacity was in agreement with the real sorption capacity achieved by quasi-second-order kinetic model. According to the R^2 values of the aforementioned models, the quasi-second-order kinetic model with higher R^2 value could better describe the behavior of phosphate ions sorption from aqueous solution using the magnetic adsorbent. Also, the results of the intra-particle diffusion model show that the adsorption mechanism includes two-steps. The adsorption rate in the first step is very fast and the adsorption rate is slow in the second step. Also, the amounts of parameter I were opposite to zero, which shows the intraparticle diffusion model is as a part of the diffusion process, although it was not the rate-controlling step. In addition, the intra-particle diffusion mechanism was not dominant during the adsorption process [41].

10. Thermodynamic Study

The thermal nature of the adsorption process (endothermic/exothermic) can be investigated through the thermodynamic study. Considering the temperature effects, the optimum temperature value can be determined to achieve maximum adsorption efficiency. Thereafter, the adsorption and equilibrium constants can be calculated. The following equations are applied to determine the adsorption

Table 4. Thermodynamic parameters for P ion adsorption on $MgO/Fe_2(MoO_4)_3$ nanocomposite

Adsorbate	Temperature (°C)	ΔG^0 (KJ/mol)	ΔH^0 (KJ/mol)	ΔS^0 (J/mol·K)
Phosphate ions	25	5.356	39.476	151.173
	30	−6.413		
	35	−7.355		
	40	−8.015		
	45	8.836		
	50	9.024		

thermodynamic factors [14,42,43].

$$\Delta G^0 = -RT\ln K_e \quad (12)$$

$$\ln(K_e) = \frac{\Delta S^0}{R} - \frac{\Delta H^0}{RT} \quad (13)$$

$$K_e = \frac{q_e}{C_e} * W \quad (14)$$

where ΔG^0, ΔS^0, ΔH^0, K_e, and W are the Gibbs free energy change (J/mol), entropy change (J/mol·K), enthalpy change (J/mol), the dimensionless equilibrium constant, and weight of adsorbent per solution volume (g/L), respectively. ΔH^0 and ΔS^0 values can be calculated from the $\ln K_e$ versus 1/T plot. Fig. S3 and Table 4 present the results of thermodynamic study in the temperature range of 25-50 °C. From these data, it can be seen that ΔG^0 values were negative; therefore, the adsorption of phosphate ions on the magnesium oxide/iron molybdate nanocomposite was spontaneous, and also ΔG^0 increased with temperature. These findings suggest that phosphate ion adsorption depends on temperature and indicates structure variations in the adsorbent and the pollutant. In addition, ΔH^0 obtained was 39.462 kJ/mol; therefore, the current adsorption process was endothermic and irreversible.

CONCLUSIONS

This study set out with the aim of assessing the adsorption capability of magnesium oxide/iron molybdate ($MgO/Fe_2(MoO_4)_3$) nanocomposite for the removal of phosphate ions from aqueous media. Several analyses,, such as SEM, EDX/Map, FTIR, XRD, TGA, BET, and TEM, were applied to characterize the synthesized adsorbent. The results demonstrated that the optimum values for pH, adsorbent dosage, temperature, time and initial ion concentration were 6 and 2 g/L, 45 °C, 80 min, and 10 mg/L, respectively. In the optimal condition, the highest removal efficiency obtained was 98.38%. Moreover, the adsorption efficiency decreased more as the result of the existence of carbonate ions in comparison with sulfate and nitrate ions. There was a competition between phosphate and carbonate ions for sitting on the magnesium oxide/iron molybdate nanocomposite sites. Furthermore, desorption studies on the synthesized adsorbent after the adsorption of phosphate ions using NaOH showed that its percentage increased with time and its maximum value was 94.84% after 1.5 hr. The current adsorbent showed an acceptable adsorption capability after four stages of adsorption/desorption process of phosphate ion. Also, Langmuir, Freundlich, and Dubinin-Radushkevich models were used to study the adsorption equilibrium; the results showed that the Freundlich isotherm model could better describe the adsorption process compared to other models. Besides, the adsorption process was physically based on the data achieved from Freundlich and Dubinin-Radushkevich models. In addition, the maximum adsorption capacity was obtained 30.21 mg/g. The kinetic behavior of the adsorption process was also described better by quasi-second-order model compared to quasi-first-order model. Finally, the thermodynamic parameters indicated that the adsorption process was endothermic and spontaneous.

CONFLICT OF INTEREST

The authors state that there is no conflict of interest in this study.

SUPPORTING INFORMATION

Additional information as noted in the text. This information is available via the Internet at http://www.springer.com/chemistry/journal/11814.

REFERENCES

1. J. Kanagaraj, T. Senthilvelan, R. C. Panda, R. Aravindhan and A. B. Mandal, *Chem. Eng. Technol.*, **37**, 1741 (2014).
2. H. Yoshida and W. A. Galinada, *AIChE J.*, **48**, 2193 (2002).
3. T. Almeelbi and A. Bezbaruah, *J. Nanopart. Res.*, **14**, 900 (2012).
4. O. Axinte, I. Volf and L. Bulgariu, *Environ. Eng. Manag. J.*, **16**, 625 (2017).
5. S. R. Habiby, H. Esmaeili and R. Foroutan, *Sep. Sci. Technol.* (2019).
6. L. Ruixia, G. Jinlong and T. Hongxiao, *J. Colloid Interface Sci.*, **248**, 268 (2002).
7. S. Y. Cho and D. K. Choi, *Korean J. Chem. Eng.*, **13**, 409 (1996).
8. D. Patureau, E. Helloin, E. Rustrian, T. Bouchez, J. P. Delgenes and R. Moletta, *Water Res.*, **35**, 189 (2001).
9. A. Adin, Y. Soffer and R. B. Aim, *Water Sci. Technol.*, **38**, 27 (1998).
10. M. Song, Z. Duan, R. Qin, X. Xu, S. Liu, S. Song, M. Zhang, Y. Li and J. Shi, *Korean J. Chem. Eng.*, **36**, 869 (2019).
11. C. Namasivayam and D. Sangeetha, *J. Colloid Interface Sci.*, **280**, 359 (2004).
12. A. B. Cundy, L. Hopkinson and R. L. Whitby, *Sci. Total Environ.*, **400**, 42 (2008).
13. Y. Abshirini, R. Foroutan and H. Esmaeili, *Mater. Res. Express*, **6**, 045607 (2019).
14. S. Abbasi, R. Foroutan, H. Esmaeili and F. Esmaeilzadeh, *Desalin.*

Water Treat., **141**, 269 (2019).
15. S. Tamjidi and H. Esmaeili, *Chem. Eng. Technol*., **42**, 607 (2019).
16. M. P. House, A. F. Carley and M. J. Bowker, *J. Catal*., **252**, 88 (2007).
17. Z. Esvandi, R. Foroutan, M. Mirjalili, G. A. Sorial and B. Ramavandi, *J. Polym. Environ*., **27**, 263 (2019).
18. J. Xiang, Q. Lin, S. Cheng, J. Guo, X. Yao, Q. Liu, G. Yin and D. Liu, *Environ. Sci. Pollut. Res*., **25**, 14032 (2018).
19. A. Ashok, L. J. Kennedy, J. J. Vijaya and U. Aruldoss, *Clean Technol. Environ*., **20**, 1219 (2018).
20. . Srirapu, A. Kumar, N. Kumari, P. Srivastava and R. N. Singh, *Int. J. Hydrogen Energy*, **43**, 16543 (2018).
21. K. Seevakan, A. Manikandan, P. Devendran, A. Baykal and T. Alagesan, *Ceram. Int*., **44**, 17735 (2018).
22. H. Hatami, A. Fotovat and A. Halajnia, *Appl. Clay Sci*., **152**, 333 (2018).
23. H. Jeon, D. J. Kim, S. J. Kim and J. H. Kim, *Fuel Process. Technol*., **116**, 325 (2013).
24. J. Feng, M. Gao, Z. Zhang, S. Liu, X. Zhao, Y. Ren, Y. Lv and Z. J. Fan, *Colloid Interface Sci*., **510**, 69 (2018).
25. A. Alayat, E. Echeverria, D. N. Mcllroy and A. G. McDonald, *Fuel Process. Technol*., **177**, 89 (2018).
26. M. Shafiee, R. Foroutan, K. Fouladi, M. Ahmadlouydarab, B. Ramavandi and S. Sahebi, *Adv. Powder Technol*., **30**, 544 (2019).
27. B. R. Vahid and M. Haghighi, *Energy Convers. Manage*., **126**, 362 (2016).
28. R. Foroutan, A. Oujifard, F. Papari and H. Esmaeili, *3 Biotech*., **9**, 78 (2019).
29. Q. Y. Yue, W. Y. Wang, B. Y. Gao, X. Xu, J. Zhang and Q. Li, *Water Environ. Res*., **82**(4), 374 (2010).
30. M. Naushad, G. Sharma, A. Kumar, S. Sharma, A. A. Ghfar, A. Bhatnagar, F. J. Stadler and M. R. Khan, *Int. J. Biol. Macromol*., **106**, 1 (2018).
31. J. Wang, Y. Liu, P. Hu and R. Huang, *Environ. Prog. Sustain*., **37**, 267 (2018).
32. S. Tamjidi, H. Esmaeili and B. K. Moghadas, *Mater. Res. Express*, **6**, 102004 (2019).
33. F. S. Sarvestani, H. Esmaeili and B. Ramavandi, *3 Biotech*., **6**, 251 (2016).
34. H. Siwek, A. Bartkowiak and M. Włodarczyk, *Water*, **11**, 633 (2019).
35. A. Robalds, L. Dreijalte, O. Bikovens and M. Klavins, *Desalin. Water Treat*., **57**, 13285 (2016).
36. L. Zeng, X. Li and J. Liu, *Water Res*., **38**, 1318 (2004).
37. A. Teimouri, H. Esmaeili, R. Foroutan and B. Ramavandi, *Korean J. Chem. Eng*., **35**, 479 (2018).
38. R. Foroutan, R. Mohammadi, S. Farjadfard, H. Esmaeili, M. Saberi, S. Sahebi, S. Dobaradaran and B. Ramavandi, *Environ. Sci. Pollut. Res*., **26**, 6336 (2019).
39. A. O. Dada, A. P. Olalekan, A. M. Olatunya and O. J. I. J. C. Dada, *IOSR-JAC*, **3**, 38 (2012).
40. H. Esmaeili and R. Foroutan, *J. Dispersion Sci. Technol*., **40**, 990 (2019).
41. M. A. P. Kelm, M. J. da Silva Júnior, S. H. de Barros Holanda, C. M. B. de Araujo, R. B. de Assis Filho, E. J. Freitas, D. R. dos Santos and M. A. da Motta Sobrinho, *Environ. Sci. Pollut. Res*., **26**, 28558 (2019).
42. N. You, X. F. Wang, J. Y. Li, H. T. Fan, H. Shen and Q. Zhang, *J. Ind. Eng. Chem*., **70**, 346 (2019).
43. Y. Liu and H. Xu, *Biochem. Eng. J*., **35**, 174 (2007).

Supporting Information

Effect of interfering ions on phosphate removal from aqueous media using magnesium oxide@ferric molybdate nanocomposite

Hossein Esmaeili*,†, Rauf Foroutan, Dariush Jafari*, and Mohammad Aghil Rezaei*****

*Department of Chemical Engineering, Bushehr Branch, Islamic Azad University, Bushehr, Iran
**Faculty of Chemical and Petroleum Engineering, University of Tabriz, Tabriz, 5166616471, Iran
***Department of Chemical Engineering, School of Chemical Engineering,
Kherad Institute of Higher Education, Bushehr, Iran
(*Received 3 November 2019 • accepted 12 January 2020*)

Equilibrium Data

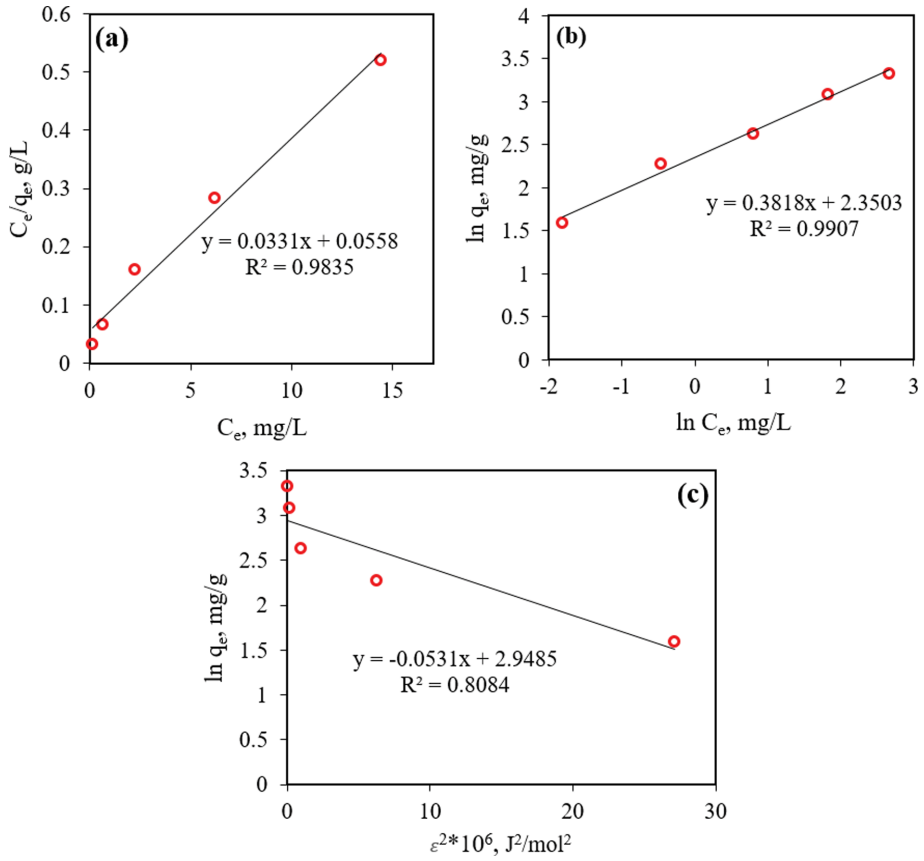


Fig. S1. Equilibrium-isotherms of P ions adsorption on $MgO/Fe_2(MoO_4)_3$ nanocomposite for (a) Langmuir, (b) Freundlich, and (c) Dubinin-Radushkevich isotherms (time=80 minutes, temperature=45 °C, sorbent dosage=2 g/L, pH=6, stirring rate=500 rpm).

Kinetic Data

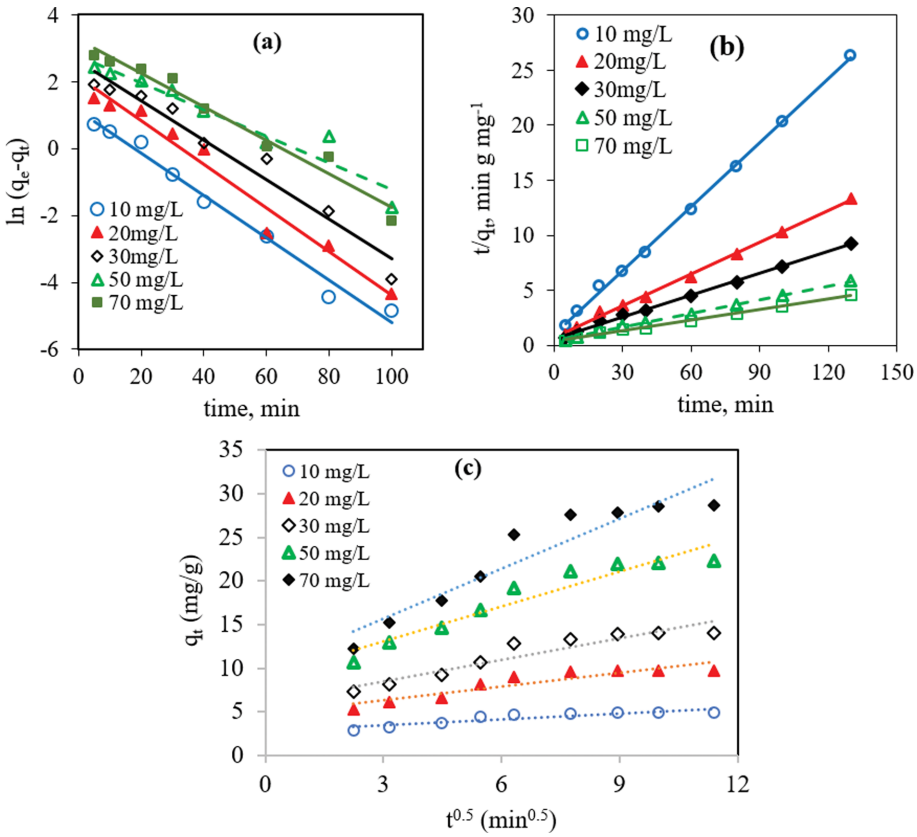


Fig. S2. (a) Quasi first-order, (b) quasi-second-order, and (c) intra-particle diffusion kinetic model plots for adsorption of P ions on magnesium oxide/iron molybdate nanocomposite (temperatureg=45 °C, sorbent dosage=2 g/L, pH=6, stirring rate=500 rpm).

Thermodynamic Study

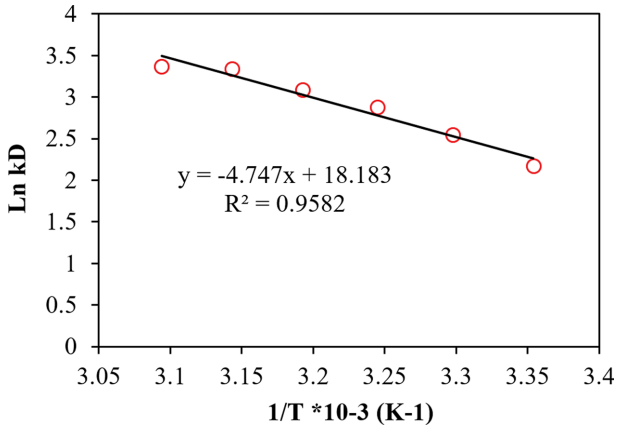


Fig. S3. Thermodynamic plot of P ions adsorption on the MgO/$Fe_2(MoO_4)_3$ nanocomposite.